SSRG International Journal of Electronics and Communication Engineering
ISSN: 2348-8549/ https://doi.org/10.14445/23488549/IJECE-V12I7P123

Volume 12 Issue 7, 295-304, July 2025

Original Article

Analysis of a Machine Learning-Assisted Perturbed Patch Antenna with Circular DGS for 6G

Prabhat Kumar Patnaik[1], Harish Chandra Mohanta[2], Ribhu Abhusan Panda[3], Dhruba C. Panda[4], M. Murali[5]

[1,2,3]*Department of Electronics and Communication Engineering, School of Engineering and Technology, Centurion University of Technology and Management, Odisha, India.*
[4]*Dhruba C. Panda, Department of Electronic Science, Berhampur University, Odisha, India.*
[5]*Department of Electronics and Communication Engineering, ACE Engineering College, Hyderabad, Telangana, India.*

[3]*Corresponding Author : ribhuabhusan.panda@cutm.ac.in*

Received: 12 May 2025 Revised: 13 June 2025 Accepted: 14 July 2025 Published: 31 July 2025

Abstract *- A compact high-frequency patch antenna with a novel flower-shaped radiating element and a circular DGS (Defected Ground Structure) is proposed for 6G and satellite communication. The radiating structure comprises two orthogonal biconvex patches with boundary-to-boundary separation equal to the guided wavelength at 15 GHz. The design attains a peak gain of 8.81 dB, a return loss of –34.388 dB, and an impedance bandwidth of 6.6 GHz, validated by fabrication on an FR4 substrate and full-wave simulations using Ansys HFSS. A mathematical derivation based on Bessel's function accurately predicts resonant frequencies, aligning closely with simulation results. In addition, a machine learning framework is developed to model S-parameter behaviour, with the Random Forest Regressor demonstrating the highest predictive accuracy (R^2 = 0.9901). The combination of electromagnetic simulation, analytical modelling, and data-driven prediction provides a robust design methodology for next-generation compact antennas.*

Keywords *- DGS, Flower-shaped patch, 6G, S_{11}, Antenna bandwidth, Antenna gain.*

1. Introduction

The leap in the evolution of wireless communication systems, ranging from 6G to satellite communications and defence applications, has necessitated a dire need for miniaturised, high-gain, and wideband antennas. Traditional patch antennas often exhibit poor impedance bandwidth and moderate gain, which limits their use in high-performance and high-frequency applications [1, 2].

To overcome these drawbacks, several improvement methods have been suggested in recent times. These consist of geometric adjustments [3], the addition of metamaterial-injected structures [4], and the application of Defected Ground Structures (DGS) to filter surface waves and enhance radiation behaviour [5-7]. Machine learning (ML) methods have recently been identified as vital tools for antenna design optimisation and performance parameter prediction, providing significant reductions in simulation time [8, 9].

While these developments have taken place, a research gap remains in integrating mathematically derived structural geometries in microstrip antenna design with data prediction using machine learning. Earlier research findings have typically focused on shape optimisation, with little research on merging mathematically driven structural innovation. Moreover, machine learning models are employed to predict key performance metrics with enhanced accuracy and efficiency.

This article proposes a new flower-shaped microstrip patch antenna, which has been mathematically designed based on two orthogonal biconvex segments with an arc-to-arc spacing equal to the guided wavelength at 15 GHz. A circular Defected Ground Structure (DGS) is incorporated into the ground plane to achieve an increased impedance bandwidth and improved radiation features.

Full-wave simulations carried out using Ansys HFSS and experimentally verified assured the performance of the antenna, having a return loss of –34.388 dB, a peak gain of 8.81 dB, and an impedance bandwidth of 6.6 GHz.This work is innovative due to the combination of mathematically driven design techniques and machine learning-based recital prediction, a relatively unseen intermingling within existing literature.

To further enhance the antenna design, a regression method based on machine learning is employed to predict the S-parameters of the antenna from its material and geometric properties. Among various models, the Random Forest

Regressor yields the best results with an R^2 score of 0.9901, underscoring the potential of AI-assisted design in future antenna systems.

2. Literature Review

Numerous research studies have investigated methods to enhance the performance of Microstrip Patch Antennas (MPAs) in terms of gain, bandwidth, and size. In this paper, Table 1 presents some of the works based on important design features like dimensional parameters, machine learning integration with MPA, operational frequency, antenna gain, and bandwidth.

Early works [10, 11] utilised Machine Learning (ML) to enhance antenna performance but lacked a mathematical framework for design based on resonant frequency. The designs achieved moderate gains of 2.06 dB and 5.62 dBi, respectively, with operating bands from sub-GHz to Ultra-Wideband (UWB). By contrast, designs [12-14] concentrated on structural improvements like Defected Ground Structures (DGS) with considerable bandwidth enrichment (e.g., 4230 MHz in [14]) but without incorporating ML or derived mathematical equations into their design.

A few other structures working in the 15 GHz band—e.g., [16-19]—obtained different levels of performance with structural adjustments such as Complementary Split-Ring Resonators (CSRR), slots, or DGS. However, previous studies have not concurrently applied mathematical analysis and machine learning to guide the design process effectively. Significantly, [20] followed an ML-based approach at 28 GHz but also without mathematical derivation for the patch geometry or resonant characteristics.

In contrast, the work presents a novel integration of analytical modelling and AI-aided optimisation. It includes a miniature 50 mm × 50 mm × 1.6 mm 15 GHz antenna with a peak gain of 8.81 dB and a wide bandwidth of 6.6 GHz. Unlike previous research, the design here is based on mathematically analysed orthogonal biconvex shapes. It utilises Random Forest Regression to predict S-parameters with high accuracy, achieving an R^2 of 0.9901.

This combined method, which is mathematical and computationally based (ML), not only fills the research gap established in previous works but also demonstrates the effective combination of predictive modelling with high-order geometric structures to achieve optimal antenna performance.

3. Antenna Design Methodology and Specifications

The antenna under consideration is constituted by two orthogonally placed biconvex radiating elements that are in a flower-like structure. The extremities of the two ends of each biconvex segment are separated arc-to-arc by the guided wavelength (λg) at 15 GHz. The antenna has dimensions of 50 mm × 50 mm × 1.6 mm, which includes an FR4 epoxy substrate with $\varepsilon r = 4.4$ and a thickness of 1.6 mm. The 0.01 mm-thick copper ground plane features a circular Defected Ground Structure (DGS) incorporated to enhance bandwidth and mitigate surface wave propagation.

The optimal radius of DGS was evaluated using parametric optimisation with the in-built toolset in Ansys HFSS, which is based on the finite element method. Simulation results indicated that the optimal DGS radius was 2 mm. The final geometric structure of the suggested design is shown in Figure 1.

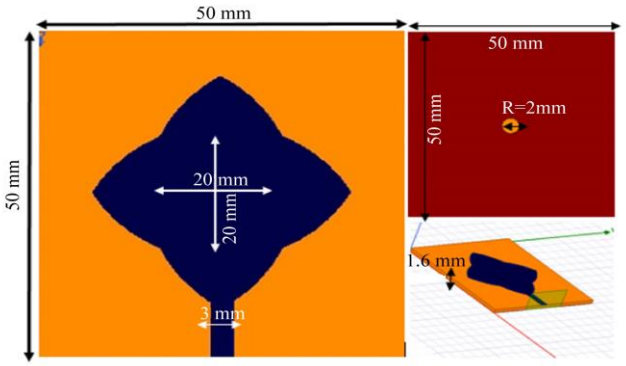

Fig. 1 Design of the flower-shaped patch

4. Mathematical Modelling of Resonant Frequencies Using Bessel Functions

Accurate analytical modelling of resonant frequencies is essential to validate the performance of microstrip patch antennas, particularly when non-standard radiating geometries are employed. The proposed flower-shaped patch antenna, consisting of orthogonal biconvex segments, is approximated as a sectorial radiating structure with circular symmetry for mathematical analysis. Considering the flow chart revealed in Figure 2, the mathematical analysis for the resonant frequency can be done.

The following equation can determine the effective dielectric constant for the proposed substrate

$$\varepsilon_{reff} = \frac{\varepsilon_r+1}{2} + \frac{\varepsilon_r-1}{2}\left\{\frac{ln\frac{\pi}{2}+\frac{1}{\varepsilon_r}ln\frac{\pi}{2}}{ln(\frac{8h}{w})}\right\} \quad (1)$$

'W' and 'h' represent the width of the feed and height of the substrate, respectively.

Similarly, the impedance of the microstrip is given by [2]

$$z_{ms} = \frac{377}{2\pi\sqrt{\frac{\varepsilon_r+1}{2}}}\left[ln\left(\frac{8h}{w}\right) + \frac{1}{8}\left(\frac{w}{2h}\right)^2 - \frac{1}{2}\frac{\varepsilon_r-1}{\varepsilon_r+1}\left\{ln\frac{\pi}{2} + \frac{1}{\varepsilon_r}ln\frac{4}{\pi}\right\}\right] \quad (2)$$

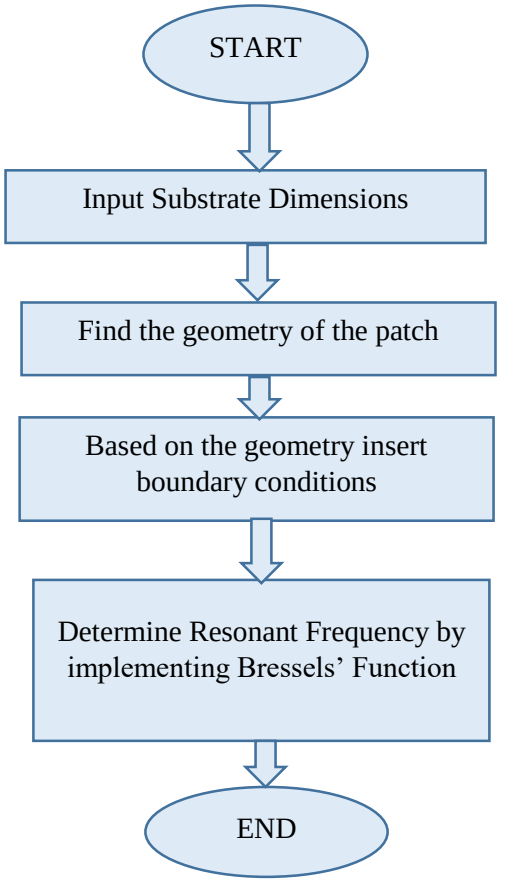

Fig. 2 Mathematical analysis flow chart

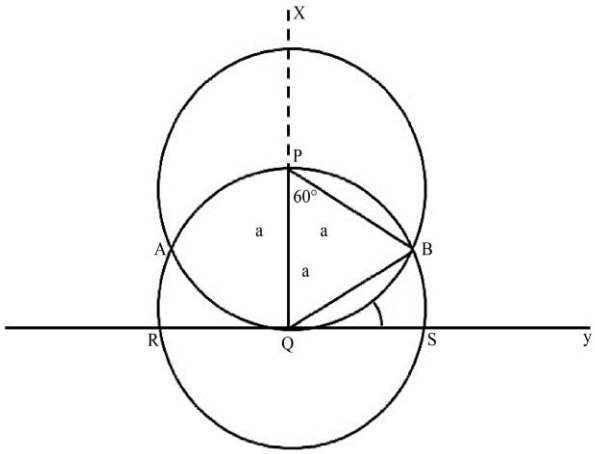

Fig. 3 Geometry for the mathematical analysis

$$\cos\theta = \frac{QS}{QB} = \frac{a}{0.5(arcAQB)} = \frac{a}{(\pi a/3)} \quad (1)$$

With a sectorial angle of 120^0 through the AQB arc

$$\theta = \cos^{-1}\frac{a}{\frac{\pi a}{3}} = \cos^{-1}\frac{3}{\pi} = 17^0 \quad (2)$$

as in Figure 3.

The patch has a curvature that can generate circular waveguides, keeping Q as its centre. Taking the boundary conditions into consideration

$$E_\rho = 0 for 0 \le \rho \le a, -\theta \le \varphi \le \pi + \theta, z = 0 \quad (3)$$

$$E_\rho = 0 for 0 \le \rho \le a, -\theta \le \varphi \le \pi + \theta, z = h \quad (4)$$

$$H_\varphi = 0 for \rho = a, -\theta \le \varphi \le \pi + \theta, 0 \le z \le h \quad (5)$$

The value of the vector potential is given by

$$A_z = BJ_m^{'}(k_\rho\rho)(A_0 \cos\varphi + B_0 Sin\varphi)A_\theta \cos K_z Z \quad (6)$$

$$J_m^{'}(k_\rho\rho) = 0 \quad (7)$$

And this is true when

$$k_\rho = \frac{x_{mn}^{'}}{a} for \rho = a \quad (8)$$

Where χ'_{mn} are the zeros of the derivative of Bessel's function.

Provided $A_0 \cos\varphi + B_0 \sin\varphi = 0$ (9)

Considering the conditional boundary values, the extreme value of "m" for ϕ=5, for which the term $(A_0 \cos\varphi + B_0 Sin\varphi)$ is zero. Based on the order, first derivatives zeros and 'n', the values are 3.8318, 7.0156, 10.1735, 13.3237 for n=1, 2, 3, 4, respectively.

Using the boundary conditions, it can be established that.

$$\frac{A_0}{B_0} = tan\, m\,\theta = -tan\{m\pi + m\theta\} \quad (10)$$

For simplicity, the first value of '*m*' (*m*=0) is acceptable.

Again, the mode of vibration depends on different values of 'n'. The maximum value of 'n' is the number of derivatives of Bessel's Function. J'_m is possible only when other terms do not become zero. Again, a maximum number of series derivations can be done up to $n \le 5$.

From equation (8),

$$\omega^2\mu\xi = \left(\frac{x_{mn}^{'}}{a}\right)^2 \quad (12)$$

$$f_{mnp} = \frac{\omega}{2\pi} = \frac{1}{2\pi\sqrt{\mu\xi}}\frac{x_{mn}^{'}}{a} \text{ or} \quad (13)$$

$$f_{mnp} = \frac{c(x_{mn}^{'})}{2\pi a\sqrt{\xi_r}} = x_{mn}^{'}(1.137) \quad (14)$$

Where $c = 3 \times 10^8\ ^m/_S$, $\xi_r = 4.4$ and a=0.02 m, the resonant frequencies are

$f_{01} = 4.358GHz$ $f_{02} = 7.978GHz$

$f_{03} = 11.566GHz$ $f_{04} = 15.148GHz$

5. Electromagnetic Simulation and Experimental Validation

The antenna was optimized using Ansys HFSS, which employs the finite element method for full-wave electromagnetic simulation. Parametric sweeps were conducted to fine-tune key design variables, including patch dimensions, feed inset width and length, and the radius of the DGS, with the objective of maximizing impedance bandwidth and gain at the target frequency of 15 GHz.

The optimized antenna was implemented on an FR4 epoxy substrate with a dielectric constant of 4.4, loss tangent of 0.02, and thickness of 1.6 mm. The patch and ground plane were etched using a standard photolithography process, and a 50-ohm impedance SMA connector was soldered for feeding. To prevent misalignment with the simulated model, fabrication tolerances were kept as low as possible to ensure accurate dimensions.

Experimental characterization was performed using a Rohde & Schwarz ZNB20 Vector Network Analyzer, which was calibrated according to the standard SOLT (Short-Open-Load-Thru) procedure. S11 return loss measurements were recorded over a 10–20 GHz frequency range in an anechoic chamber. The simulated return loss of -35.76 dB is well approximated by the measured values, which show a minimum return loss of -30.388 dB at 15 GHz. Both testing and simulation confirm that the impedance bandwidth of the antenna is larger than 6.6 GHz, namely from 12.2 GHz to 18.8 GHz. Figure 4 shows the experimental setup and the realized antenna.

Fig. 4 Experimental setup for measurement

The radiation patterns were measured in the far-field region using a standard antenna measurement setup. The simulated peak gain was 8.96 dB, while the measured peak gain was 8.81 dB, indicating close alignment of the values. Minor discrepancies between the simulation and measurement can be attributed to fabrication imperfections, SMA connector losses, and slight dielectric inhomogeneities in the substrate material. A close correlation between simulated and experimental results validates the design methodology, confirming that the combination of a flower-shaped radiating geometry and optimised DGS significantly improves the return loss, antenna gain, and bandwidth. This confirms the antenna's applicability for compact high-frequency systems such as 6G communications, satellite links, and radar applications.

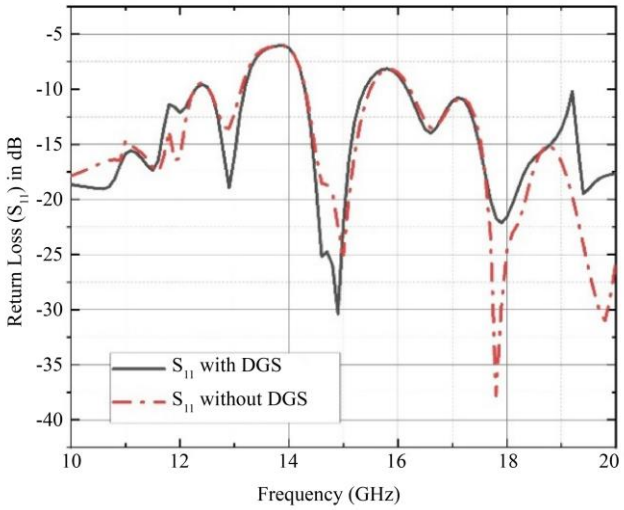

Fig. 5 S-Parameter Comparison

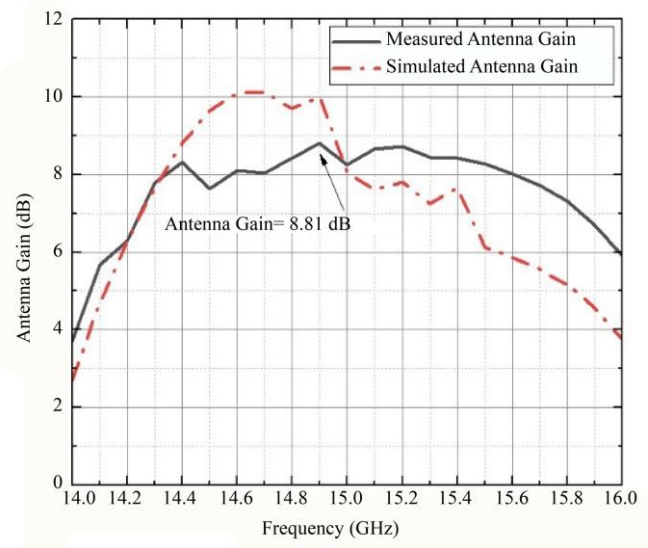

Fig. 6 Antenna Gain Comparison

The comparison plots of S-parameter and antenna gain are depicted in Figures 5 and 6, respectively. Table 1 includes antenna parameter comparisons.

Table 1. Comparison of simulated and measured performance parameters

Parameters	Simulated With DGS	Simulated Without DGS	Measured With DGS	% error
Antenna Gain (dB)	9.98	8.05	8.81	8.6
S_{11} (dB)	-30.388	-25.07	-34.388	27
Radiation efficiency (%)	83.57	89.03	92.57	3.8
Resonant Frequency (GHz)	14.9	15	14.91	0.6

Table 2. Comparison of the performance of various regression models

Model	MAE (%)	MSE (%)	MAPE (%)	RMSE (%)	R-squared (%)
Support Vector Regression	2.8991	20.6783	0.2072	4.5473	0.1543
Random Forest Regressor	0.3038	0.2431	0.0211	0.4931	0.9901
Gradient Boosting Regressor	0.1985	0.1127	0.0155	0.3357	0.9954
K-Nearest Neighbor Regressor	0.6683	1.3172	0.0474	1.1477	0.9461
Polynomial Regressor	3.2687	20.2348	0.2641	4.4983	0.1725

6. Machine Learning-Based Prediction and Model Performance Analysis

Machine Learning (ML) methods have been found to be practical tools for optimising antenna design efficiency by predicting performance parameters, such as return loss (S11), thereby eliminating the need for iterative full-wave simulations. This work employed a supervised regression method to simulate the S11 behaviour of the antenna under consideration.

The workflow for the machine learning–assisted prediction is illustrated in Figure 7. The process begins with dataset generation, where key antenna parameters, including patch dimensions, feed position, and DGS radius, are systematically varied using parametric sweeps in Ansys HFSS. The corresponding simulated S11 values across the 10–20 GHz frequency range were extracted to form the training dataset.

Data preprocessing was performed to normalise feature values and eliminate any outliers that could adversely impact model training. Following this, multiple regression algorithms were evaluated, including the various algorithms mentioned in Table 2. Hyperparameter tuning was conducted via a grid search combined with five-fold cross-validation to ensure model generalisation and prevent overfitting.

Table 2 offers a comparative overview of model performance in the regression models. In the models compared, the Random Forest Regressor registered the highest level of predictive accuracy, with a Mean Absolute Error (MAE) of 0.3038%, a Root Mean Squared Error (RMSE) of 0.4931%, and a coefficient of determination (R^2) of 0.9901. Figures 8 and 9 provide the corresponding bar graphs of model-wise error measures and accuracy levels, respectively.

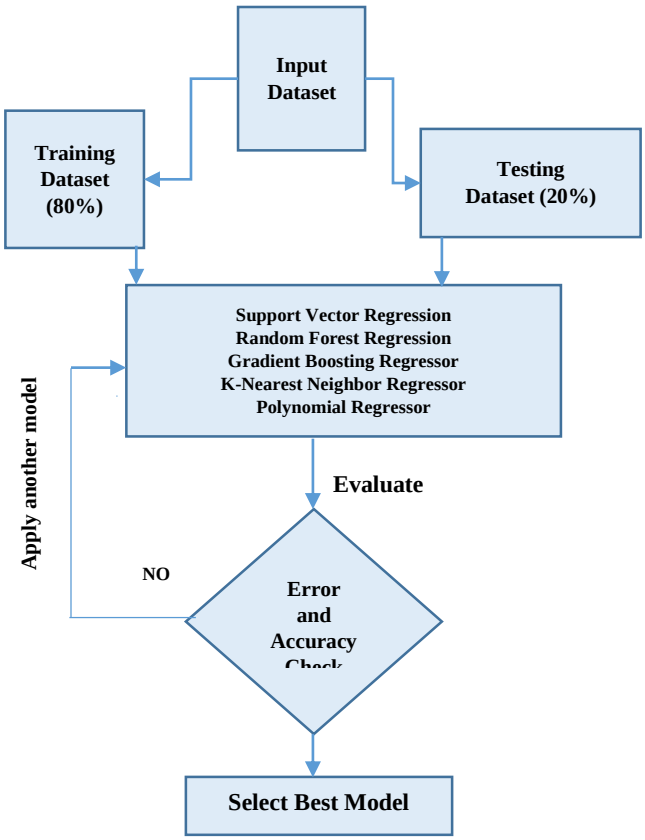

Fig. 7 The flowchart for the machine learning approach

A comparison between the predicted and simulated S11 curves using different models across various evaluation metrics is illustrated in Figures 10-14.

The results demonstrate that machine learning models, particularly the Random Forest Regressor, can accurately predict the antenna's S-parameter behavior, significantly reducing design iteration time. The integration of data-driven prediction into the antenna design workflow highlights the potential for developing intelligent, rapid optimization frameworks for next-generation high-frequency antenna systems.

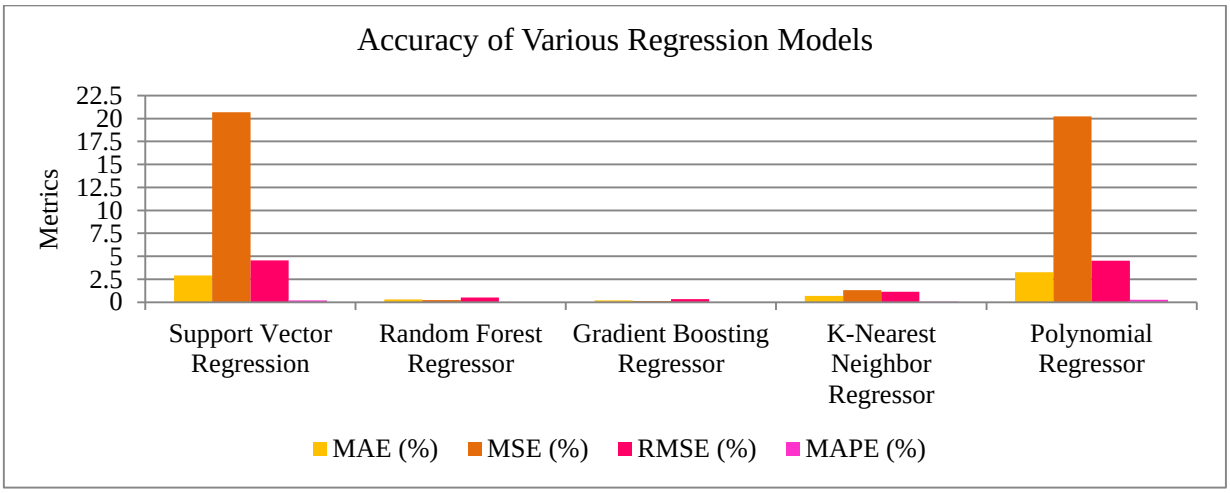

Fig. 8 Bar charts of errors for different algorithms

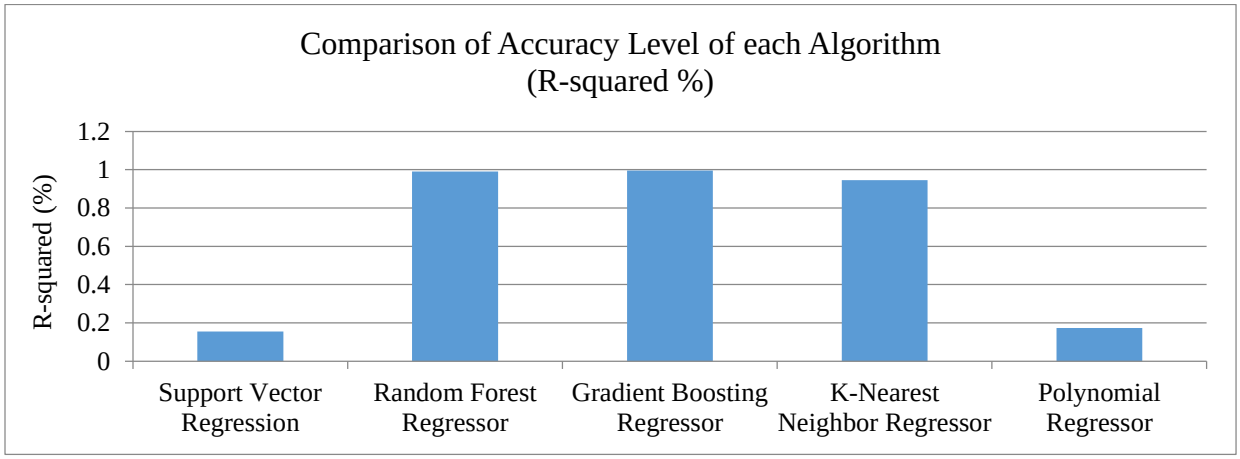

Fig. 9 Bar charts of the accuracy levels of each algorithm

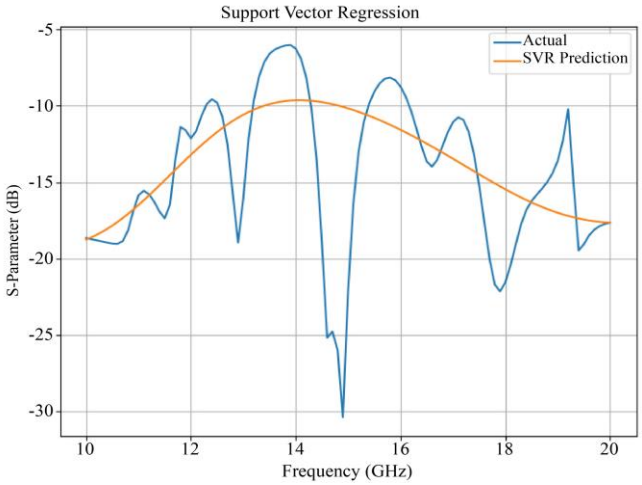

Fig. 10 Analysis of S-parameter plot by support vector regression

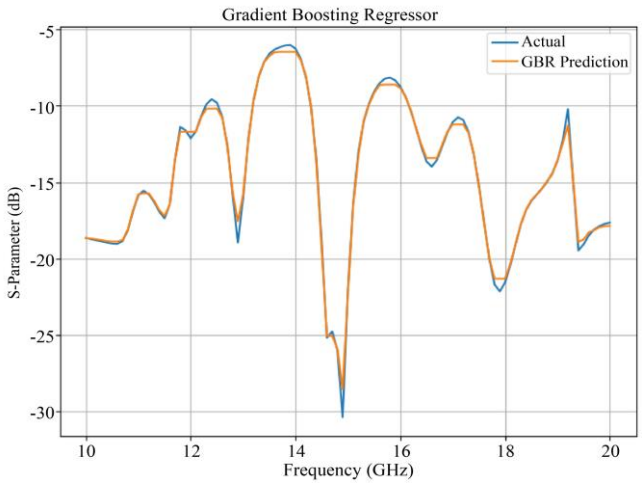

Fig. 11 Analysis of S-parameter plot by gradient boosting regressor

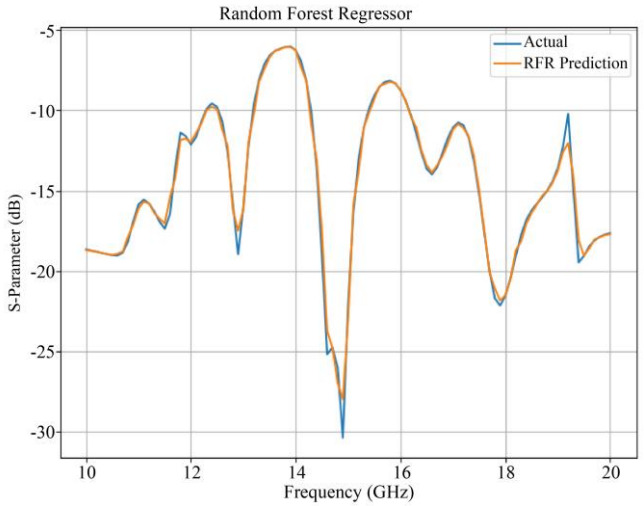

Fig. 12 Analysis of S-parameter plot by random forest regressor

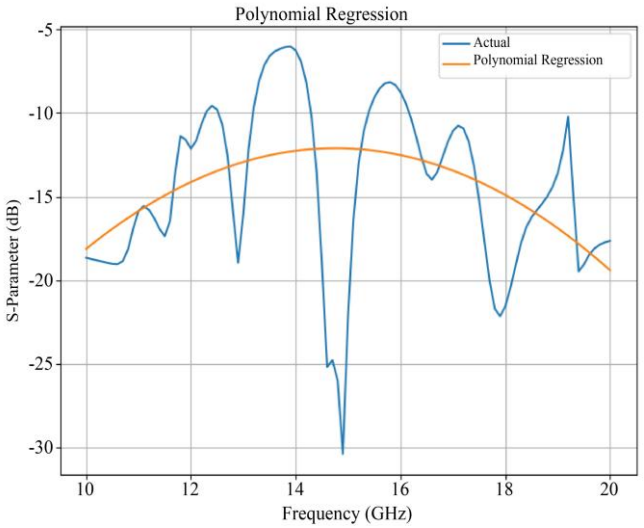

Fig. 13 Analysis by polynomial regression

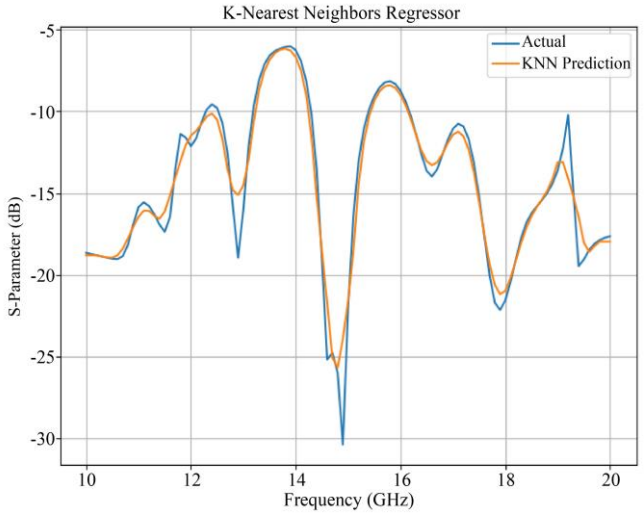

Fig. 14 Comparison of S-parameter between the measured result and the predicted models

7. Reasonable Study with State-of-the-Art Designs

To compare the performance of the suggested antenna with a circular Defected Ground Structure, a comparative analysis was conducted with contemporary microstrip antenna designs at the same or nearby frequency bands. A tabulation of comparative performance factors, including return loss, impedance bandwidth, peak gain, and physical size, is provided in Table 3.

The antenna in question offers a maximum gain of 8.81 dB and an impedance bandwidth of 6.6 GHz, in addition to a measured return loss of –34.388 dB. The antenna in this work outperforms previous configurations, such as semi-circular patches [3], perturbed slots [6], and metamaterial-based structures [10], in terms of bandwidth and gain. In particular, the bandwidth enhancement exceeds 200% in some cases, attributed to the integration of the circular DGS, which effectively suppresses surface currents and extends the impedance bandwidth. Furthermore, the novel flower-shaped geometry increases effective aperture utilisation without increasing the footprint (50 mm × 50 mm), offering a better gain-to-size ratio compared to existing designs. Additionally, most prior works did not incorporate data-driven design or modelling. In contrast, this work integrates a machine learning–based predictive framework, which accelerates the design cycle and achieves high prediction accuracy (R^2 = 0.9901) for return loss behaviour—an advancement not addressed in comparable studies. In summary, the findings confirm that the proposed antenna offers improved performance in terms of gain, impedance bandwidth, and predictive modelling accuracy, making it suitable for high-end applications such as 6G wireless systems, satellite communications, and miniaturised radar platforms. The Voltage Standing Wave Ratio (VSWR), a crucial measure of impedance matching, was analysed using a terminated transmission line model. The presented antenna has a VSWR of 1.06, which is extremely close to the theoretical value of unity, as shown in Figure 15.

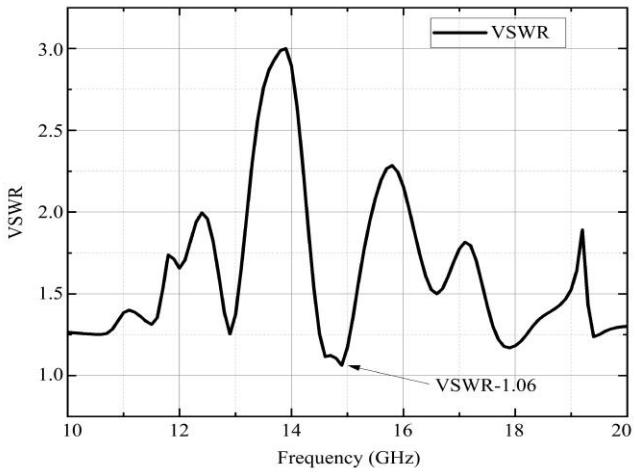

Fig. 15 VSWR of the proposed model

Table 3. Comparison of the proposed antenna with existing state-of-the-art designs in terms of bandwidth, gain, and physical size

References	Dimension of the Antenna	Mathematical analysis for resonant frequency	Machine Learning Approach	Frequency of operation	Gain	Additional Technique	Bandwidth
[10]	80 mm × 60 mm × 0.5 mm	NO	YES	868 MHz- 915 MHz	2.06 dB	MPA/Slot	47 MHz
[11]	42.6 mm × 42.4 mm × 1.6 mm	NO	YES	0.48 GHz-7.84 GHz	5.62 dBi	Square Slot	multiband
[12]	$0.8\lambda_0 \times 0.8\lambda_0 \times 0.03\lambda_0$ (λ_0: free-space wavelength at 6 GHz)	NO	NO	6GHz	4 dBi	DGS	1 GHz
[13]	$0.32\ \lambda_0 \times 0.32\ \lambda_0 \times 0.006\ \lambda_0$ (λ_0: free-space wavelength at 2.4 GHz)	NO	NO	2.42 GHz, 2.5 GHz	2.3 dBi	DGS	135 MHz
[14]	74 mm × 74 mm × 44 mm	NO	NO	4.69GHz-8.92 GHz	9.98 dB	DGS	4230 MHz
[15]	21.04 mm × 27.66 mm ×1.6 mm	NO	YES	3.3GHz	4.06 dB.	NO	100 MHz
[16]	26 X 27 X 1.6mm^3	NO	NO	14.84	6.44 dBi	CSRR and DGS	15 GHz
[17]	24 mm × 15 mm × 1.524 mm	NO	NO	15 GHz	NA	DGS	1.04 GHz
[18]	100 mm × 43 mm ×1.575 mm	NO	NO	14.50 to 15.25 GHz	9.61 dB	H-Slot	750 MHz
[19]	8 mm × 9.5 mm × 1.6 mm	NO	NO	15 GHz	3.488	Multiple Slot	1.14 GHz
[20]	10 mm×10 mm×0.251mm	NO	YES	28GHz	7.63	None	0.658 GHz
Proposed Work	50 mm × 50 mm × 1.6 mm	YES	YES	15 GHz	8.81	DGS	6.6 GHz

The designed antenna exhibits a radiation efficiency of 92.57% and, as measured by simulated directivity and realised gain, values of 8.81 dB, reflecting extremely efficient radiative performance. Figure 16 presents the three-dimensional far-field radiation pattern, which includes symmetrical lobes. Figure 17 also presents the surface current distribution, which indicates strong and uniform current flow over the radiating structure, thereby substantiating the effective excitation of the patch and its suitability for high-frequency usage.

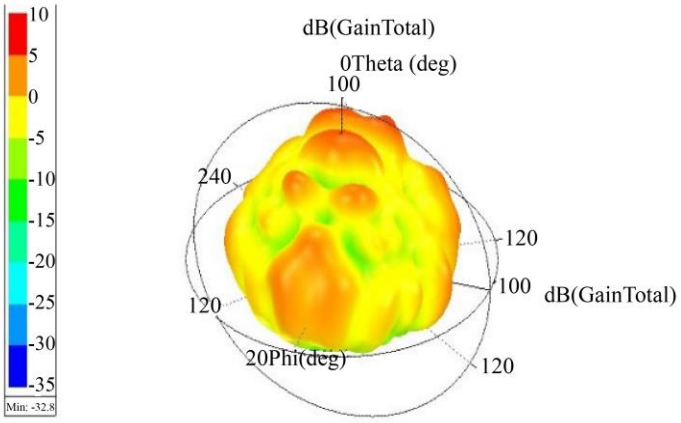

Fig. 16 3D radiation pattern

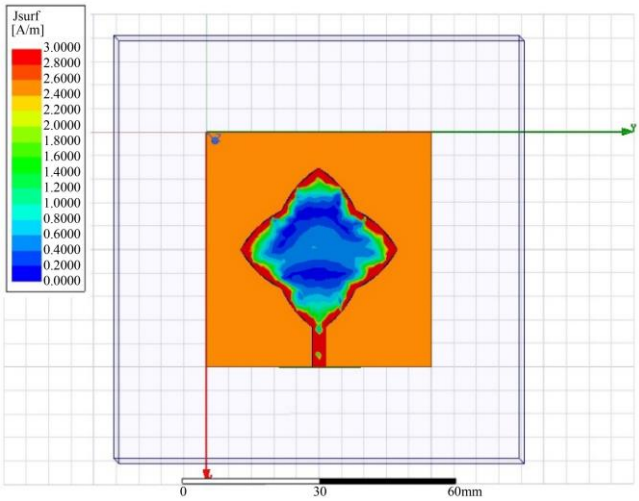

Fig. 17 Distribution of Current on selected surface

8. Conclusion

This study presents the design, analysis, and machine learning–assisted performance modelling of a miniaturized flower-shaped microstrip patch antenna integrated with a circular Defected Ground Structure (DGS), targeting high-frequency applications such as 6G communication systems. The novel radiating structure, composed of orthogonal biconvex segments, effectively enhanced the aperture efficiency while maintaining a compact dimension. The incorporation of the circular DGS significantly improved the antenna's impedance bandwidth and return loss characteristics.

Full-wave electromagnetic simulations and fabricated measurements confirmed the antenna's high performance, achieving a measured return loss of –34.388 dB, a peak gain of 8.81 dB, and an impedance bandwidth of 6.6 GHz centred around 15 GHz. A mathematical analysis using Bessel function modelling accurately predicted resonant frequencies, closely matching simulation and measurement results.

Furthermore, a machine learning–based regression framework, utilising a Random Forest Regressor, achieved an R^2 score of 0.9901, demonstrating effective prediction of S-parameters and significantly reducing reliance on iterative full-wave simulations. The integration of innovative antenna geometry, optimised ground-plane engineering, mathematical modelling, and ML-based predictive analysis establishes a comprehensive framework for advanced antenna development.

References

[1] Priyanka Garg, and Priyanka Jain, "Isolation Improvement of MIMO Antenna Using a Novel Flower Shaped Metamaterial Absorber at 5.5 GHz WiMAX Band," *IEEE Transactions on Circuits and Systems II: Express Briefs*, vol. 67, no. 4, pp. 675-679, 2019. [CrossRef] [Google Scholar] [Publisher Link]

[2] Ayush Tripathi, Athul O Asok, and Sukomal Dey, "Brain Tumor Detection with Flower Shaped Monopole Antennas utilizing Microwave Imaging," *2023 IEEE Microwaves, Antennas, and Propagation Conference*, Ahmedabad, India, pp. 1-6, 2023. [CrossRef] [Google Scholar] [Publisher Link]

[3] Amiya Kumar Mondal et al., "Miniature Planar Log Periodic Dipole Array Antenna for IEMI Detection Application," *IEEE Transactions on Electromagnetic Compatibility*, vol. 66, no. 5, pp. 1307-1314, 2024. [CrossRef] [Google Scholar] [Publisher Link]

[4] S. Pravesh et al., "Study and Design of Heart-Shaped Microstrip Patch Antenna for SART Applications," *Results in Engineering*, vol. 25, pp. 1-10, 2025. [CrossRef] [Google Scholar] [Publisher Link]

[5] Nafis Almas Nafi et al., "A Novel Theta-Shaped Slotted Patch Antenna with a Unique DGS for Sub-6 GHz 5G Communication," *Results in Engineering*, vol. 24, pp. 1-10, 2024. [CrossRef] [Google Scholar] [Publisher Link]

[6] Golak Santra, and Piyush N. Patel, "Horizontally Polarized Omnidirectional Antenna Using Slotted Rectangular Patch and Defected Ground Structure," *IEEE Antennas and Wireless Propagation Letters*, vol. 22, no. 4, pp. 704-708, 2022. [CrossRef] [Google Scholar] [Publisher Link]

[7] Ajay Singh, and Sunil Joshi, "Design of Y-Shaped Tri-Band Rectangular slot DGS Patch Antenna at Sub-6 GHz Frequency Range for 5G Communication," *Journal of Engineering and Applied Science*, vol. 71, pp. 1-17, 2024. [CrossRef] [Google Scholar] [Publisher Link]

[8] K.V. Prasad, and Venkata Siva Prasad Makkapati, "Investigation of Slotted Ground and M-Shaped DGS in Enhancing MIMO Antenna Isolation," *Wireless Personal Communications*, vol. 136, pp. 2027-2045, 2024. [CrossRef] [Google Scholar] [Publisher Link]

[9] Garima Singh et al., "An Innovative DGS Based Textile Antenna with Semi-Circular Slot for Future IoT's and AI Applications," *Transactions on Electrical and Electronic Materials*, vol. 26, pp. 78-103, 2025. [CrossRef] [Google Scholar] [Publisher Link]

[10] Gagandeep Kaur et al., "Dual Port UWB MIMO Dielectric Resonator Antenna (DRA) with Airplane Shaped Defective Ground Plane (DGS) with Improved Isolation Level," *Wireless Personal Communications*, vol. 139, pp. 1225-1237, 2024. [CrossRef] [Google Scholar] [Publisher Link]

[11] Mohamed I. Waly et al., "Optimization of a Compact Wearable LoRa Patch Antenna for Vital Sign Monitoring in WBAN Medical Applications Using Machine Learning," *IEEE Access*, vol. 12, pp. 103860-103879, 2024. [CrossRef] [Google Scholar] [Publisher Link]

[12] Kanhaiya Sharma, and Ganga Prasad Pandey, "Efficient Modelling of Compact Microstrip Antenna Using Machine Learning," *AEU - International Journal of Electronics and Communications*, vol. 135, 2021. [CrossRef] [Google Scholar] [Publisher Link]

[13] Deepak Kumar Naik et al., "CMA Approach for a DGS-Based Wideband Circular Patch Antenna With Low Cross Polarization," *IEEE Antennas and Wireless Propagation Letters*, vol. 22, no. 3, pp. 586-590, 2023. [CrossRef] [Google Scholar] [Publisher Link]

[14] Shengjie Chen et al., "A Wideband Quad-Port 3-D MIMO Antenna Decoupled With DGS Structure for Roadside Units," *IEEE Antennas and Wireless Propagation Letters*, vol. 24, no. 3, pp. 616-620, 2025. [CrossRef] [Google Scholar] [Publisher Link]

[15] Vinod Babu Pusuluri, A.M. Prasad, and Naresh K. Darimireddy, "Decision-Tree Based Machine Learning Approach for the Design and Optimization of 5G n78 Sub-Band Antenna for WiMAX/WLAN Applications," *2023 IEEE Wireless Antenna and Microwave Symposium*, Ahmedabad, India, pp. 1-4, 2023. [CrossRef] [Google Scholar] [Publisher Link]

[16] P. Mohith Kumar et al., "A Leaf Shaped Patch Antenna for Wideband Applications," *2023 IEEE Wireless Antenna and Microwave Symposium*, Ahmedabad, India, pp. 1-5, 2023. [CrossRef] [Google Scholar] [Publisher Link]

[17] B.G. Hakanoglu, O. Sen, and M. Turkmen, "A Square Microstrip Patch Antenna with Enhanced Return Loss Through Defected Ground Plane for 5G Wireless Networks," *2018 2nd URSI Atlantic Radio Science Meeting (AT-RASC)*, Gran Canaria, Spain, pp. 1-4, 2018. [CrossRef] [Google Scholar] [Publisher Link]

[18] Adhie Surya Ruswanditya, Yuyu Wahyu, and Heroe Wijanto, "MIMO 8×8 Antenna with Two H-Slotted Rectangular Patch Array for 5G Access Radio at 15 GHz," *2017 International Conference on Control, Electronics, Renewable Energy and Communications*, Yogyakarta, Indonesia, pp. 221-226, 2017. [CrossRef] [Google Scholar] [Publisher Link]

[19] Mekala Harinath Reddy et al., "Design of Microstrip Patch Antenna with Multiple Slots for Satellite Communication," *2017 International Conference on Communication and Signal Processing*, Chennai, India, pp. 0830-0834, 2017. [CrossRef] [Google Scholar] [Publisher Link]

[20] Md. Sohel Rana, Sheikh Md. Rabiul Islam, and Sanjukta Sarker, "Machine Learning Based on Patch Antenna Design and Optimization for 5 G Applications at 28GHz," *Results in Engineering*, vol. 24, pp. 1-14, 2024. [CrossRef] [Google Scholar] [Publisher Link]